Correlated Membrane Fluctuations in Nanocrystal Superlattices

Brian A. Korgel

Department of Chemical Engineering and Texas Materials Institute, and Center for Nano- and Molecular Science and Technology, The University of Texas, Austin, Texas 78712-1062

(Received 14 April 2000)

Superlattices of organic monolayer-stabilized silver nanocrystals exhibit structural integrity at temperatures well above the melting point of the hydrocarbon capping ligands (i.e., the C_8, C_{12}, and C_{16} alkanethiols used in this study). Temperature-dependent small angle x-ray scattering reveals that topological disordering occurs with spatially correlated domains of characteristic length ξ that grow with increasing temperature until ξ diverges at a critical temperature T_c, as $\xi \sim \xi_0(1 - T/T_c)^{-0.67}$. A power law analysis of the scattering intensity with wave vector indicates that interactions between membranes due to thermal undulations control the topology below T_c.

DOI: 10.1103/PhysRevLett.86.127 PACS numbers: 68.35.Rh, 61.46.+w

Surface fluctuations are largely responsible for the broad diversity of phase behavior exhibited by solutions of amphiphilic molecules [1,2]. Hydrophobic interactions orient amphiphiles into monolayers or bilayers, and it is this *two-dimensional* organization that produces the morphological polymorphism common to surfactant solutions. These noncovalently connected surfaces are flexible with low bending constants k; they undergo thermal fluctuations, which give rise to steric interactions that stabilize either isotropic phases, such as micelles or vesicles, or phases with random two-dimensional surfaces, such as the L_α (lamellar) and L_3 (sponge) phases [1,3,4]. In the bidimensional phases, the thermal fluctuations tend to spatially *correlate* neighboring planar structures. However, the thermal fluctuations also *disrupt* long-range orientational order—leading to the formation of continuous crumpled membranes of randomly connected plaquettes, with a characteristic persistance length ξ_K [5]. Nonetheless, the repulsive forces (e.g., $V_{\text{und}} = [3\pi^2(k_BT)^2/128k](1/r^2)$ [3]) can lead to repetitive membrane-membrane separations significantly larger than the membrane thickness itself, as in the swollen lamellar and sponge phases, for example [1]. In these systems, it is the combination of amphiphilic organization into membranes and flexibility of the membranelike structures that give rise to complex surface topologies [6].

Organic monolayer-passivated silver nanocrystals consist of a metal core coated by an adsorbed layer of alkanethiol capping ligands [7–11]. The thiol binds strongly to the silver surface, leaving the hydrocarbon exposed to the surrounding medium. The hydrocarbon layer controls particle size and solubility, and provides a steric barrier to particle aggregation, thus, playing a role similar to the stabilizing micellar surfactant that coats the water droplets in water-in-oil microemulsions. Like other colloidal systems, nanocrystals self-assemble into a variety of mesoscopic structures, and have been promoted as "building blocks" for constructing new materials and devices with dimensions far below those possible using existing techniques [8–12]. For example, nanocrystals with very narrow size distributions can be self-assembled into organized superlattices by evaporating the solvent from a dispersion placed on a substrate [8–13]. Superlattice *formation* depends on a combination of interparticle and molecular chain-chain interactions [8–15]. However, the superlattice could be considered as a cubic surfactant phase with inorganic cores occupying lattice (hole) positions [9]. The small angle x-ray scattering (SAXS) data presented in this Letter show that correlated thermal fluctuations of capping ligand *membranes* determine the temperature dependence and topology of the thermal induced order-disorder phase transition of silver nanocrystal superlattices. The thermal undulations of the capping ligand membranes lead to a self-avoiding random surface with spatially correlated domain sizes that grow as the temperature increases.

Silver nanocrystals were prepared with three different capping ligand chain lengths ($C_{12}H_{25}SH$, $C_8H_{17}SH$, and $C_{16}H_{33}SH$) [9,11]. The size distributions were narrowed using an antisolvent size fractionation step [11]. Figure 1 shows typical TEM images and SAXS data from the nanocrystals used in this study. Nanocrystals with a standard deviation about the mean diameter of $\pm 5\%$ form an ordered nanocrystal superlattice, whereas, size distributions greater than approximately $\pm 12\%$ disrupt superlattice formation and allow only short-range order [11]. Sharp Bragg diffraction peaks appear from the ordered superlattice, whereas the SAXS pattern for the disordered film resembles that of a fluid. Both organized and disordered nanocrystal films were studied to determine if the nanocrystal organization affects the thermal stability of the superlattice.

In SAXS, the scattering intensity $I(q)$ [where $q = (4\pi/\lambda)\sin(\theta/2)$, with θ as the scattering angle, and $\lambda = 1.54$ Å] relates proportionally to the shape factor for individual nanocrystals $P(qR)$, and the static structure factor $S(q)$: $I(q) \propto P(qR)S(q)$ [16,17]. To determine the average nanocrystal radius $\overline{R}$ and size distribution, $P(qR)$ was measured using dilute nanocrystal dispersions in hexane, where $S(q) = 1$ [9,11,16,18]. $P(qR)$ for a sphere is $P(qR) = 3[\sin(qR) - qR\cos(qR)/(qR)^3]^2$

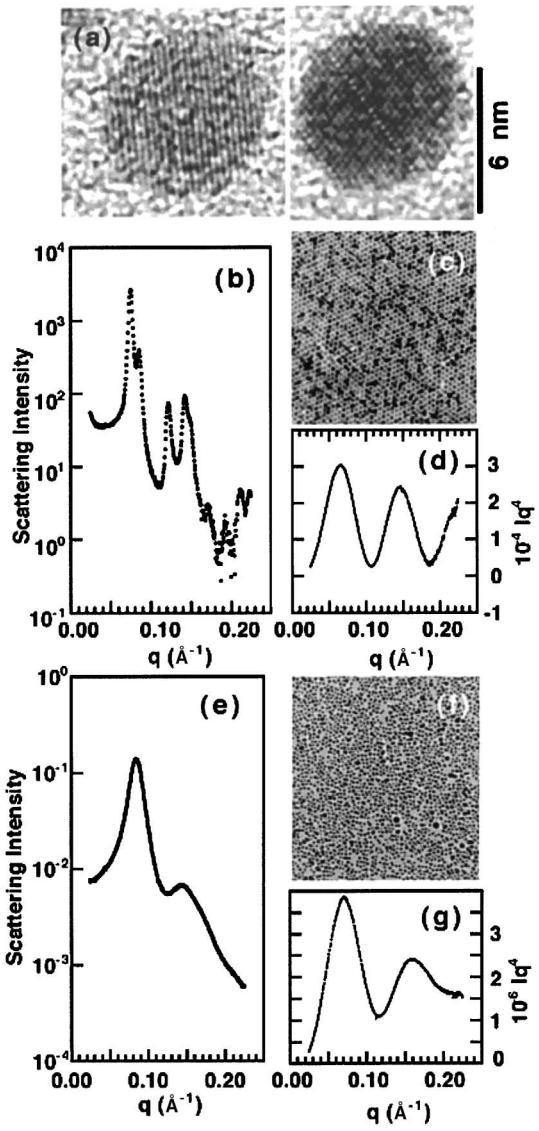

FIG. 1. (a) High resolution TEM images of two dodecanethiol-capped silver nanocrystals, each oriented differently on a carbon substrate. (b) SAXS from dodecanethiol-capped silver nanocrystals ($R = 41 \pm 2.8$ Å) indexes to an fcc superlattice ($d_{111} = 84.8$ Å; interparticle separation, $\delta_{SL} = 15.9$ Å). (c) TEM and (d) SAXS for hexane-dispersed particles. (e) SAXS and (f) TEM for condensed "polydisperse" nanocrystals ($R = 36 \pm 5.2$ Å); the nearest neighbor separation δ is 18 Å. (g) SAXS of hexane-dispersed nanocrystals. The SAXS data in (d) and (g) are fit with Eq. (1). TEM images were obtained using either a JEOL JEL-2000 EX electron microscope with point-to-point resolution of 0.3 nm, or a JEOL 2010 transmission electron microscope with 1.7 Å point-to-point resolution, operating with a 200 kV accelerating voltage.

[16]. A Gaussian size distribution, $n(R)/n_{\text{total}}$, with an average particle radius $\overline{R}$, and standard deviation σ, $[n(R)/n_{\text{total}}] = (1/\sigma\sqrt{2\pi})\exp[-(R - \overline{R})^2/2\sigma^2]$ was assumed for all fits, where [8,16]

$$I(q) \propto \int_0^\infty \left(\frac{n(R)}{n_{\text{total}}}\right) P(qR) R^6 \, dR \,. \qquad (1)$$

Figures 1(d) and 1(g) show $P(qR)$ measured for monodisperse and polydisperse dodecanethiol-capped silver nanocrystals, respectively (1 mg/ml). These curves are characteristic of noninteracting particles [9] and were fit with Eq. (1) to determine $\overline{R}$ and σ (Table I).

Figure 2 shows the temperature-dependent SAXS intensity profiles of arrays of nanocrystals capped with C_8, C_{12}, and C_{16} alkanes [19]. SAXS measurements were collected in one minute frames with the sample temperature increased by 5 °C/min using a specially designed differential scanning calorimetry sample holder (Linkham THM)

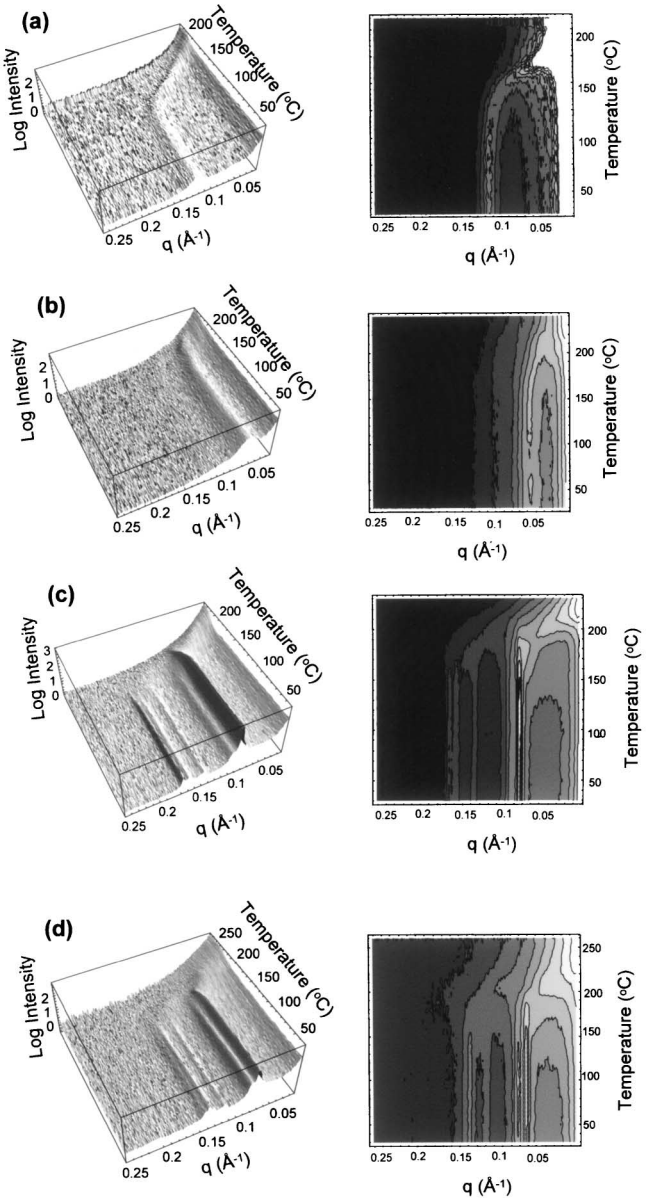

FIG. 2. Temperature-dependent SAXS measurements on "polydisperse" C_8 [(a) $R = 20 \pm 2.4$ Å] and C_{16} [(b), $R = 38 \pm 6.5$ Å] capped silver nanocrystals and "monodisperse" C_{12}-capped [(c), $R = 35 \pm 3.2$ Å; (d), $R = 41 \pm 2.8$ Å] nanocrystals. The column of plots on the right-hand side is the corresponding contour plot of the data on the left-hand side.

TABLE I. Values obtained from Figs. 3 and 4. The subscripts 1 and 2 on the constants ν and ξ_0 represent values below and above the crossover temperature T_x, respectively. The error for η and ν was determined from a least squares fit of the data in Figs. 3 and 4.

Sample	Hydrocarbon chain length	R (Å)	η	T_c (°C)	T_x (°C)	ν_1	ν_2	$\xi_{0.1}$ (Å)	$\xi_{0.2}$ (Å)	$\Lambda = \frac{4\xi_{0.1}}{R}$
(a)	8	20 ± 2.4	1.38 ± 0.03	193 ± 1	160	0.47	0.64 ± 0.03	21.8	14.8	4.36
(b)	16	38 ± 6.5	1.39 ± 0.01	300 ± 2	165	0.20	0.66 ± 0.04	86.9	41.1	9.15
(c)	12	35 ± 3.2	1.33 ± 0.03	228 ± 2	185	0.24	0.66 ± 0.05	48.6	16.1	5.55
(d)	12	41 ± 2.8	1.36 ± 0.06	260 ± 2	190	0.25	0.64 ± 0.04	60.9	25.4	5.94

[20]. This temperature scan rate was sufficiently slow to eliminate any apparent kinetic effects during structural reorganization [18]. In all of the samples, the first order diffraction peak disappears within a relatively narrow temperature window, indicating the onset of topological disorder. The diffraction peaks broaden substantially near this transition temperature due to much enhanced thermal vibrations of the nanocrystals in the lattice [18]. In this narrow temperature range, disordering of the nanocrystal array resembles the melting of an atomic solid as reported in Ref. [18]. However, above this temperature a clear distinction between the melting of an atomic solid and a nanocrystal array appears.

In all of the superlattice samples, when the temperature rises above the "melting" temperature, a new diffraction peak appears at slightly lower q than the (111) diffraction peak. This new scattering domain has a characteristic size ξ, related to q, $\xi = 2\pi/q$. The peak intensity gradually increases with temperature, and shifts to lower q, indicating the formation of a bicontinuous phase with spatially correlated domains much larger than either the capping ligand thickness or the nanocrystal diameter [1]. The temperature dependence of the domain size is plotted in Fig. 3. At a critical temperature T_c, ξ diverges [21]. T_c is much higher than the melting temperature of the capping ligands, much less than silver core melting temperatures, and increases with increasing chain lengths. With increasing temperature, ξ grows as $\xi \sim \xi_0(1 - T/T_c)^{-\nu}$. Table I shows the values of the measured critical exponent ν. There appears to be a crossover temperature T_x, where ν increases. For the C_8-capped nanocrystals below T_x, ν is close to the mean-field value of 0.5, indicative of separated (yet correlated) growing domains of clusters [22].

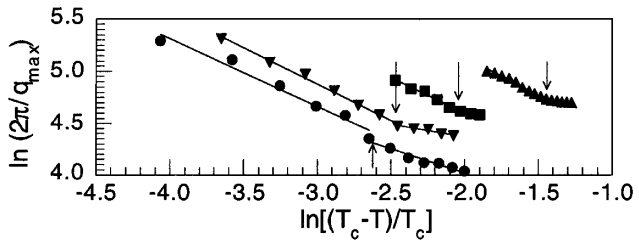

FIG. 3. Plot of $\ln[(T_c - T)/T_c]$ vs $\ln(2\pi/q)$, where q is $q_{\max}$ for the scattering data in Fig. 2 for samples C_8 (●), C_{16} (▲), C_{12} (41 Å) (■), and C_{12} (35 Å) (▼). The arrows indicate the crossover temperature T_x for each sample.

The C_{16} and C_{12}-capped nanocrystals exhibit $\nu < 0.5$. T_x varies with capping ligand chain length and slightly with nanocrystal size. Above T_x, however, all of the samples exhibit ν typical of Ising behavior ($\nu = 0.63$) [22]. Below T_x, $\xi_{0,1}$ is on the order of a nanocrystal radius, whereas, above T_x, $\xi_{0,2}$ decreases to the characteristic length of the capping ligand layer thickness.

A reduced range of interaction, described by the parameter, $\Lambda = 4\xi_0/R$, is related to the crossover from classical to Ising behavior [22]. Greater interaction range should appear as a larger value of Λ, and a crossover from mean-field behavior to Ising behavior is expected when Λ is much greater than 1, as is certainly the case in these systems (see Table I). When Λ is much greater than 1, values of ν less than the mean-field value of 0.5 are possible at temperatures below T_x. In these studies, Λ was higher for longer hydrocarbon chains and affected the values of ν accordingly.

The bicontinuous phase behavior at temperatures below T_c is consistent with a sponge phase, which is stabilized by long-range entropic forces due to the thermal fluctuations of capping ligand "membranes" [3]. Prior to melting, hydrocarbon chains are attached to the silver cores, which force their side-by-side arrangement [9]. As the temperature rises above the superlattice melting temperature, the silver cores aggregate to form metal clusters surrounded by hydrocarbon chains. Within the nanocrystal clusters, surfactant remains (i.e., there is no unoccupied space); however, many of the chains displace to the interface separating the clusters of nanocrystals. The van der Waals attractions between chains will help to maintain their alignment at this interface. It is the undulations of this interfacial membrane—consisting of the soft hydrocarbon ligands—that stabilize the sponge phase. Therefore, phase transition temperatures should depend on the bending rigidity of the membranes. Significantly stiffer membranes are expected from C_{16} hydrocarbons than the shorter chain C_{12} and C_8 hydrocarbon chains, due to the differences in van der Waals attractions between chains. Increased stiffness should lead to higher T_c, as is indeed observed.

Stemming from the Landau-Peierls effect [23], the steric interactions produced by thermal undulations of *fluid* membranes lead to a long-range algebraic decay of correlations [3,24]. In the vicinity of the first order diffraction peak, this results in the power law scaling of the scattering intensity as a function of q, $S(q) \sim (q - q_{\max})^{-(2-\eta)}$.

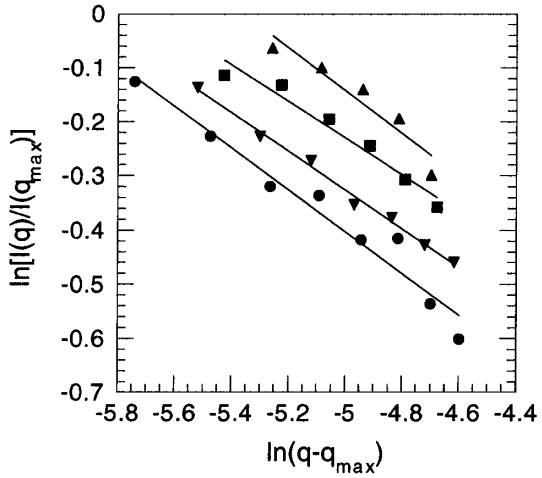

FIG. 4. Plot of $\ln[I(q)/I(q_{\max})]$ vs $\ln(q - q_{\max})$, where $q_{\max}$ is the wave vector at the scattering peak in Fig. 2 for samples C_8 at 185 °C (●); C_{16} at 210 °C (▲); C_{12} at 215 °C (41 Å) (■); and C_{12} at 215 °C (35 Å) (▼). The curves represent the best fit lines to determine η.

Figure 4 shows representative determinations of η for these samples. Characteristic of the universal nature of undulation interactions, the critical exponent is approximately $\frac{4}{3}$ for all of the samples studied [1,3,24].

The SAXS measurements here reveal that thermal undulations of capping ligand membranes in nanocrystal superlattices lead to spatially correlated random surfaces. The noncovalent interactions of the inorganic cores and the surrounding sea of ligands play a major role in determining the thermal stability of the superlattice, as this study has shown, and gives rise to phase behavior analogous to that of surfactant solutions at ambient conditions.

B. K. gratefully acknowledges helpful discussions with D. Fitzmaurice and N. Zaccheroni, and the assistance of B. E. Komanschek. This work was supported in part by DuPont, the NSF, and the Welch Foundation.

[1] For a recent review, see D. Roux, C. R. Safinya, and F. Nallet, in *Micelles, Membranes, Microemulsions, and Monolayers,* edited by W. M. Gelbart, A. BenShaul, and D. Roux (Springer-Verlag, New York, 1994), and references therein.

[2] *Statistical Mechanics of Membranes and Surfaces,* edited by D. Nelson, T. Piran, and S. Weinberg (World Scientific, Singapore, 1989).

[3] W. Helfrich, Z. Naturforsch **33A**, 305 (1978).

[4] M. E. Cates, D. Roux, D. Andelman, S. T. Milner, and S. A. Safran, Europhys. Lett. **5**, 733 (1988).

[5] P. G. de Gennes and C. Taupin, J. Chem. Phys. **86**, 2294 (1982).

[6] See, for example, G. Gompper and D. M. Kroll, Phys. Rev. Lett. **81**, 2284 (1998), and references therein.

[7] M. Brust, M. Walker, D. Bethell, D. J. Schiffrin, and R. Whyman, J. Chem. Soc. Chem. Commun. **1994**, 801 (1994); D. V. Leff, P. C. Ohara, J. C. Heath, and W. M. Gelbart, J. Phys. Chem. **99**, 7036 (1995).

[8] B. A. Korgel and D. Fitzmaurice, Phys. Rev. Lett. **80**, 3531 (1998).

[9] B. A. Korgel, S. Fullam, S. Connolly, and D. Fitzmaurice, J. Phys. Chem. B **102**, 8379 (1998).

[10] R. L. Whetten, M. N. Shafigullin, J. T. Khoury, T. G. Schaaff, I. Vezmar, M. M. Alvarez, and A. Wilkinson, Acc. Chem. Res. **32**, 397 (1999).

[11] B. A. Korgel and D. Fitzmaurice, Phys. Rev. B **59**, 14 191 (1999).

[12] B. A. Korgel and D. Fitzmaurice, Adv. Mater. **10**, 661 (1998).

[13] S. Connolly, S. Fullam, B. Korgel, and D. Fitzmaurice, J. Am. Chem. Soc. **120**, 2969 (1998).

[14] W. D. Luedtke and U. Landman, J. Phys. Chem. **100**, 13 323 (1996).

[15] P. C. Ohara, D. V. Leff, J. R. Heath, and W. M. Gelbart, Phys. Rev. Lett. **75**, 3466 (1995).

[16] *Small-Angle X-ray Scattering,* edited by O. Glatter and O. Kratky (Academic Press, New York, 1982).

[17] SAXS measurements were conducted on beam line 8.2 of the Synchrotron Radiation Source at the Daresbury Laboratory, Warrington, U.K. [13]. Scattered photons were collected on a multiwire gas-filled quadrant detector. The scattering angle was calibrated using an oriented specimen of wet collagen (rat tail tendon). The incident radiation intensity was recorded using a parallel plate ionization detector located before the sample cell. All experimental data were corrected for background scattering, sample absorption, and the positional alinearity of the detector.

[18] B. A. Korgel, N. Zaccheroni, and D. Fitzmaurice, J. Am. Chem. Soc. **121**, 3533 (1999).

[19] The nanocrystal arrays were formed by evaporation onto mica substrates as thick films. Condensed nanocrystal films exhibit reproducible d spacing and superstructure, supporting that these films represent equilibrium structures. A ^{1}H NMR spectrum of the nanocrystals in chloroform-d confirmed that all dodecanethiol present in solution was adsorbed at the silver nanocrystal surface, and Fourier-transform infrared spectroscopy and elemental analysis showed that the thiol head groups close pack on the nanocrystal surface.

[20] W. Bras, G. E. Derbyshire, A. Devine, S. M. Clark, J. Cooke, B. E. Komanschek, and A. J. Ryan, J. Appl. Crystallogr. **28**, 26 (1995).

[21] The critical phase transition likely stems from hydrocarbon and metal core phase segregation, perhaps through the formation of clusters of metal cores embedded ligands analogous to a micellar "droplet" phase in surfactant solutions.

[22] M. E. Fisher, Phys. Rev. Lett. **57**, 1911 (1986).

[23] J. M. Ziman, *Models of Disorder* (Cambridge University Press, New York, 1979).

[24] Strictly speaking, this analysis holds for liquid crystals with the smectic A structure [1]. However, the steric interactions between membranes are expected to be the same in the sponge phase and the correlations should exhibit an algebraic decay near the critical point [i.e., the Ornstein-Zernike result, $g(r) \sim \exp(-R/\xi)/R$ [22]]. In general, $\eta = 4/3(1 - \delta/\xi)$ when undulation interactions stabilize the bidimensional structure. Since $\xi \gg \delta$ in Fig. 4, $\eta = \frac{4}{3}$ indicates steric stabilization of this sponge phase.